Biomedical Optics EXPRESS

Improved localization accuracy in stochastic super-resolution fluorescence microscopy by K-factor image deshadowing

Tali Ilovitsh,[1] Amihai Meiri,[1] Carl G. Ebeling,[2] Rajesh Menon,[3] Jordan M. Gerton,[2] Erik M. Jorgensen,[4] and Zeev Zalevsky[1,*]

[1]*Faculty of Engineering, Bar-Ilan University, Ramat-Gan 52900, Israel*
[2]*Department of Physics and Astronomy, University of Utah, Salt Lake City, UT USA*
[3]*Department of Electrical and Computer Engineering, University of Utah, Salt Lake City, UT USA*
[4]*Department of Biology and Howard Hughes Medical Institute, University of Utah, Salt Lake City, UT USA*
[*] *zalevsz@eng.biu.ac.il*

Abstract: Localization of a single fluorescent particle with sub-diffraction-limit accuracy is a key merit in localization microscopy. Existing methods such as photoactivated localization microscopy (PALM) and stochastic optical reconstruction microscopy (STORM) achieve localization accuracies of single emitters that can reach an order of magnitude lower than the conventional resolving capabilities of optical microscopy. However, these techniques require a sparse distribution of simultaneously activated fluorophores in the field of view, resulting in larger time needed for the construction of the full image. In this paper we present the use of a nonlinear image decomposition algorithm termed K-factor, which reduces an image into a nonlinear set of contrast-ordered decompositions whose joint product reassembles the original image. The K-factor technique, when implemented on raw data prior to localization, can improve the localization accuracy of standard existing methods, and also enable the localization of overlapping particles, allowing the use of increased fluorophore activation density, and thereby increased data collection speed. Numerical simulations of fluorescence data with random probe positions, and especially at high densities of activated fluorophores, demonstrate an improvement of up to *85%* in the localization precision compared to single fitting techniques. Implementing the proposed concept on experimental data of cellular structures yielded a *37%* improvement in resolution for the same super-resolution image acquisition time, and a decrease of *42%* in the collection time of super-resolution data with the same resolution.

OCIS codes: (180.2520) Fluorescence microscopy; (100.0100) Image processing; (100.3010) Image reconstruction techniques; (100.6640) Superresolution;

References and links

1. P. van Roessel and A. H. Brand, "Imaging into the future: visualizing gene expression and protein interactions with fluorescent proteins," Nat. Cell Biol. **4**(1), E15–E20 (2002).
2. A. S. Belmont, "Visualizing chromosome dynamics with GFP," Trends Cell Biol. **11**(6), 250–257 (2001).
3. W. T. Dempster, "Principles of microscope illumination and the problem of glare," J. Opt. Soc. Am. **34**(12), 695–710 (1944).
4. L. Rayleigh, "XV. On the theory of optical images, with special reference to the microscope," London, Edinburgh, Dublin Philos. Mag. J. Sci. **42**(255), 167–195 (1896).
5. E. Abbe, "Beitrage zur theorie des mikroskops und der mikroskopischen Wahrnehmung," Arch. Für Mikroskopische Anat. **9**(1), 413–418 (1873).
6. E. Betzig, G. H. Patterson, R. Sougrat, O. W. Lindwasser, S. Olenych, J. S. Bonifacino, M. W. Davidson, J. Lippincott-Schwartz, and H. F. Hess, "Imaging intracellular fluorescent proteins at nanometer resolution," Science **313**(5793), 1642–1645 (2006).

#198546 - $15.00 USD Received 30 Sep 2013; revised 20 Nov 2013; accepted 21 Nov 2013; published 16 Dec 2013

7. E. Betzig, J. K. Trautman, T. D. Harris, J. S. Weiner, and R. L. Kostelak, "Breaking the diffraction barrier: optical microscopy on a nanometric scale," Science **251**(5000), 1468–1470 (1991).
8. K. Braeckmans, D. Vercauteren, J. Demeester, and S. C. De Smedt, "Nanoscopy and multidimensional optical fluorescence microscopy," in (Chapman and Hall, 2010).
9. H. Shroff, C. G. Galbraith, J. A. Galbraith, and E. Betzig, "Live-cell photoactivated localization microscopy of nanoscale adhesion dynamics," Nat. Methods **5**(5), 417–423 (2008).
10. M. J. Rust, M. Bates, and X. Zhuang, "Sub-diffraction-limit imaging by stochastic optical reconstruction microscopy (STORM)," Nat. Methods **3**(10), 793–796 (2006).
11. S. T. Hess, T. P. K. Girirajan, and M. D. Mason, "Ultra-high resolution imaging by fluorescence photoactivation localization microscopy," Biophys. J. **91**(11), 4258–4272 (2006).
12. N. Bobroff, "Position measurement with a resolution and noise-limited instrument," Rev. Sci. Instrum. **57**(6), 1152 (1986).
13. R. J. Ober, S. Ram, and E. S. Ward, "Localization accuracy in single-molecule microscopy," Biophys. J. **86**(2), 1185–1200 (2004).
14. L. A. Shepp and Y. Vardi, "Maximum likelihood reconstruction for emission tomography," IEEE Trans. Med. Imaging **1**(2), 113–122 (1982).
15. A. Yildiz, J. N. Forkey, S. A. McKinney, T. Ha, Y. E. Goldman, and P. R. Selvin, "Myosin V walks hand-over-hand: single fluorophore imaging with 1.5-nm localization," Science **300**(5628), 2061–2065 (2003).
16. M. P. Gordon, T. Ha, and P. R. Selvin, "Single-molecule high-resolution imaging with photobleaching," Proc. Natl. Acad. Sci. U.S.A. **101**(17), 6462–6465 (2004).
17. R. E. Thompson, D. R. Larson, and W. W. Webb, "Precise nanometer localization analysis for individual fluorescent probes," Biophys. J. **82**(5), 2775–2783 (2002).
18. R. Henriques, C. Griffiths, E. Hesper Rego, and M. M. Mhlanga, "PALM and STORM: unlocking live-cell super-resolution," Biopolymers **95**(5), 322–331 (2011).
19. F. Huang, S. L. Schwartz, J. M. Byars, and K. A. Lidke, "Simultaneous multiple-emitter fitting for single molecule super-resolution imaging," Biomed. Opt. Express **2**(5), 1377–1393 (2011).
20. A. Sergé, N. Bertaux, H. Rigneault, and D. Marguet, "Dynamic multiple-target tracing to probe spatiotemporal cartography of cell membranes," Nat. Methods **5**(8), 687–694 (2008).
21. X. Qu, D. Wu, L. Mets, and N. Scherer, "Nanometer-localized multiple single-molecule fluorescence microscopy," in *Proceedings of the National Academy of Sciences of the United States of America* (2004), pp. 11298–11303.
22. E. A. Mukamel, H. Babcock, and X. Zhuang, "Statistical deconvolution for superresolution fluorescence microscopy," Biophys. J. **102**(10), 2391–2400 (2012).
23. R. P. J. Nieuwenhuizen, K. A. Lidke, M. Bates, D. L. Puig, D. Grünwald, S. Stallinga, and B. Rieger, "Measuring image resolution in optical nanoscopy," Nat. Methods **10**(6), 557–562 (2013).
24. J. L. Johnson and J. R. Taylor, "K-Factor Image Factorization," in *AeroSense'99. International Society for Optics and Photonics* (1999), Vol. 3715, pp. 166–174.
25. G. Pavlovic and A. Tekalp, "Restoration in the presence of multiplicative noise with application to scanned photographic images," Acoust. Speech. Signal **90**, 1913–1916 (1990).
26. A. Toet, "Multiscale contrast enhancement with applications to image fusion," Opt. Eng. **31**(5), 1026 (1992).
27. J. L. Johnson and M. L. Padgett, "PCNN models and applications," IEEE Trans. Neural Netw. **10**(3), 480–498 (1999).
28. J. L. Johnson, M. L. Padgett, and W. A. Friday, "Multiscale image factorization," Proc. Int. Conf. Neural Networks **3**, 1465–1468 (1997).
29. J. L. Johnson and J. R. Taylor, "Image factorization : a new hierarchical decomposition technique," Opt. Eng. **38**(9), 1517–1523 (1999).
30. R. Juskaitis, "Measuring the real point spread function of high numerical aperture microscope objective lense," in *Handbook of Biological Confocal Microscopy*, J. B. Pawley, ed. (Springer, 2006), pp. 239–250.
31. B. Zhang, J. Zerubia, and J. C. Olivo-Marin, "Gaussian approximations of fluorescence microscope point-spread function models," Appl. Opt. **46**(10), 1819–1829 (2007).
32. J. R. Janesick, *Scientific Charge Coupled Devices* (SPIE Press monograph, 2001), pp. 605–419.
33. J. C. Waters, "Accuracy and precision in quantitative fluorescence microscopy," J. Cell Biol. **185**(7), 1135–1148 (2009).
34. M. K. Cheezum, W. F. Walker, and W. H. Guilford, "Quantitative comparison of algorithms for tracking single fluorescent particles," Biophys. J. **81**(4), 2378–2388 (2001).
35. R. N. Ghosh and W. W. Webb, "Automated detection and tracking of individual and clustered cell surface low density lipoprotein receptor molecules," Biophys. J. **66**(5), 1301–1318 (1994).
36. D. L. Snyder, C. W. Helstrom, A. D. Lanterman, M. Faisal, and R. L. White, "Compensation for readout noise in CCD images," J. Opt. Soc. Am. A. **12**(2), 272–283 (1995).
37. M. D. Abràmoff, J. M. Paulo, and J. R. Sunanda, "Image processing with ImageJ," Biophotonics Int. **11**, 36–42 (2004).
38. R. Henriques, M. Lelek, E. F. Fornasiero, F. Valtorta, C. Zimmer, and M. M. Mhlanga, "QuickPALM: 3D real-time photoactivation nanoscopy image processing in ImageJ," Nat. Methods **7**(5), 339–340 (2010).
39. N. Banterle, K. H. Bui, E. A. Lemke, and M. Beck, "Fourier ring correlation as a resolution criterion for super-resolution microscopy," J. Struct. Biol. **183**(3), 363–367 (2013).

#198546 - $15.00 USD Received 30 Sep 2013; revised 20 Nov 2013; accepted 21 Nov 2013; published 16 Dec 2013

1. Introduction

Fluorescence microscopy is the most popular technique used in biological imaging applications [1,2] due to the capabilities to target and modify specific single proteins within the host organism. However, the resolution of a visible light microscope is limited by the phenomenon of diffraction [3] to length scales set by the Rayleigh criterion to approximately half the wavelength of the light [4,5]. Due to this limitation, any object smaller than the microscope resolution will appear as a diffraction-limited spot with a point spread function (PSF) given by an Airy function. The desire to observe biological structures and functions at length scales smaller than the diffraction limit has led to the development of super-resolution techniques that enable imaging intracellular structures with sub-diffraction-limit accuracy [6–8].

Single molecule localization microscopy techniques, such as PALM [9] and STORM [10], use optical control to activate a sparse subset of fluorescently tagged proteins in which the PSF of each individual activated fluorophore does not overlap with that of its nearest activated neighbor. This allows for the determination of the position of individual probes to a much higher accuracy than conventional optical methods. The cycle of activation, imaging, and photobleaching is repeated until all the fluorophores are exhausted, or a sufficient number of them have been localized, and the measured molecular positions are then plotted to generate a composite image [11].

In super-resolution microscopy, ultraprecise localization is usually accomplished by fitting the diffraction-limited image of individual fluorophores to an ideal PSF using algorithms such as non-linear least squares [12,13], and maximum likelihood [14]. These methods can provide precision down to *~10nm*, limited primarily by the number of photons collected from each particular fluorophore [15,16], and have been used to great effect in single particle tracking as well as in other imaging related applications. In these techniques, reliable localization of a single fluorescent molecule requires both a sufficient number of photons (*N*) in the measured PSF, and that the activated molecules be spatially separated by a distance greater than several times the width of their PSFs [17]. Overlapping PSFs in standard localization algorithms are generally discarded; this requires that the activation density remain low across the field of view, which increases the composite image acquisition time [18]. To address this problem, several methods have been recently developed with the aim of localizing overlapping PSFs. One utilizes a maximum likelihood technique with increasing numbers of point sources within the recorded PSF in the localization algorithm and is built for graphics processing unit (GPU) analysis, and as such is relatively fast – the analysis time is on the order of minutes [19–21]. Another paper uses a statistical deconvolution technique that iterates through the observed PSF with a guess-work of overlapping PSFs. This approach is very slow and requires *~10* times more computation *time/frame* than the other methods of single-emitter fitting [22].

The problem of overlapping PSFs in super-resolution microscopy also affects the ultimate spatial resolution of the composite image. In particular, the achievable spatial resolution is determined by the localization density (i.e., the density of successfully localized spots) in addition to the precision of each localization [17,18,23]. Using conventional localization algorithms, when the number of photons emitted by the fluorophore is relatively low or the spots are closely spaced, the localization density decreases since many regions of interest (ROI: areas on the image that map to actual fluorophore locations on the sample) are discarded in the analysis. Thus, high localization precision, high labeling density, and near-unity localization efficiency of those fluorescent labels are all needed to achieve the best possible spatial resolution. Here, we demonstrate a nonlinear image-factorization algorithm designed for two distinct but related purposes: to suppress image noise associated with low signal levels (poor photon statistics) and to differentiate image features associated with different contrast levels. This approach increases spatial resolution and image acquisition

#198546 - $15.00 USD Received 30 Sep 2013; revised 20 Nov 2013; accepted 21 Nov 2013; published 16 Dec 2013

speed both by requiring fewer photons to achieve the same localization precision and by allowing for a higher density of activated fluorophores during each acquisition cycle.

The aim of this algorithm is effectively to sharpen the edges of the PSF from a single point source. This sharpening will simultaneously allow isolated fluorophores to be localized with higher precision (for a given number of photons), and two overlapping fluorophores to be effectively isolated such that each can be localized to high precision. Usually, spatial denoising techniques can be divided into linear and nonlinear approaches [24]. Mean and Wiener filters [25] are two classical linear solutions which simply mask an image using the local statistical measurements of pixels. At the same time, they also blur the edge. On the contrary, nonlinear filtering technologies have the advantages to preserve the edge and fine details. One such method is a multiscale renormalization algorithm which produces a fused image by nonlinear recombination of the ratio of low-pass (ROLP) pyramidal decompositions of the original images [26]. Another method is a cyclic algorithm for shadow removal based on pulse-coupled neural networks (PCNN), an image processing algorithm derived from biologically-grounded cortical models that addressed the experimental findings of stimulus-induced synchronous bursts of pulse activity [27,28]. The PCNN-based factorization is an efficient image-processing tool for noise smoothing and elementary image segmentation that operates on local image patches. However, these methods are mathematically intractable and have a high computational complexity. The adopted method is a non-linear algorithm, which improves contrast at the PSF edges without increasing spurious noise. In particular, our method uses the K-factor transformation, which decomposes the image into hierarchical contrast-ordered factors whose joint product reconstructs the original pattern [29]. The K-factor decomposition divides the image pattern into factors where noise elements are distinct from those containing the image structure of interest. In this decomposition, the first few components, which have the highest contrast depth, contain mainly the desired image information while the higher orders contain mostly noise components. The K-factor algorithm is applied to raw image data prior to emitter localization, and does not add much computational complexity nor processing time, requiring only fractions of a millisecond per frame. Furthermore, the proposed method reduces the total number of individual frames that are required for the reconstruction of the final image, thus reducing the overall computation time.

The paper is organized as follows: First, the theoretical background for imaging single molecules, the mathematical background for nonlinear filtering algorithms, and the K-factor transform are presented. Second, numerical simulations for a variety of parameters inherent in the K-factor algorithm are presented and fully discussed. Third, the proposed algorithm is applied on experimentally acquired images to validate the approach.

2. Theoretical background

For an aberration-free imaging system, the diffraction-limited point spread function corresponding to a single point emitter (i.e. fluorescent label) is given by an Airy function [30]. Near the peak, this function is approximated by a Gaussian, which is mathematically simpler [31]. The measured intensity of the diffraction limited spot is given by the acquired data together with photon shot-noise, background noise created most commonly by out-of-focus fluorescence, charge coupled device (CCD) readout noise, dark current, and extraneous fluorescence in the microscope. The model for the intensity at (x,y) of a fluorescent particle located at (x_0,y_0), is given by [17]:

$$I(x,y) = \frac{N}{2\pi\sigma^2} e^{-\frac{(x-x_0)^2+(y-y_0)^2}{2\sigma^2}} + \eta_B \pm \eta_{shot} \quad (1)$$

where N is the total number of photons collected from the fluorophores' label by the image acquisition system during the measurement period, σ is the standard deviation of the

#198546 - $15.00 USD Received 30 Sep 2013; revised 20 Nov 2013; accepted 21 Nov 2013; published 16 Dec 2013

Gaussian, that is given by setting the e^{-1} point of the intensity model to be equal to the Rayleigh radius, η_B is a Poisson distributed random variable with variance N_b that describes the background noise (assumed constant across the field of view), and η_{shot} is a Poisson distributed random variable that describes the shot noise with a mean equal to the square root of the total intensity in each pixel [32]. In the absence of aberrations, the values will be equal and given by [33]:

$$\sigma = \frac{0.6 \times \lambda}{\sqrt{2}\text{N.A.}} \tag{2}$$

where N. A. is the numerical aperture of the objective and λ is the wavelength of the emitted light.

In existing localization microscopy methods, the assumption is that two fluorophores must be spatially well separated to achieve minimal penetration of the tails of one PSF into the other. The detection of each PSF is accomplished by establishing an intensity threshold value that distinguishes background from signal and determining whether a certain PSF exceeds this value. If so, the data is fit to a model of a Gaussian profile with a single peak. If the two PSFs are in close proximity such that the saddle between them is higher than the threshold, they will be indistinguishable and be considered as one, resulting in an increased localization error. To mitigate these errors, ROIs exhibiting elongated (asymmetric) intensity profiles are often discarded from the sample set, effectively reducing the sampling density. Thus, the ability to reduce the saddle between two overlapping PSFs will allow for fewer discarded point sources in the localization algorithm, while also allowing for faster data acquisition rates.

3. K-factor algorithm

The K-factor algorithm is an image factorization [24,29] technique, which reduces an image into a nonlinear finite or infinite set of contrast-ordered pseudoimage factors whose joint product reassembles the original image.

The K-factor transformation of an image *I(x,y)* can be described mathematically as:

$$\mathrm{I}(\mathrm{x},\mathrm{y}) = \prod_{\mathrm{n}=1}^{M} \mathrm{f}_{\mathrm{n}}(\mathrm{x},\mathrm{y}) \tag{3}$$

where M is the number of factors that reconstruct the image, and f_n are the pseudo image factors that when multiplied together reconstruct the image and are given by:

$$\mathrm{f}_{\mathrm{n}}(\mathrm{x},\mathrm{y}) = \frac{1+\mathrm{k}^{\mathrm{n}}\mathrm{g}_{\mathrm{n}}(\mathrm{x},\mathrm{y})}{1+\mathrm{k}^{\mathrm{n}}} \tag{4}$$

where the parameter k controls the contrast depth at each level with a value is between *0* and *1*, and g_n is a binary image computed as:

$$g_n(x,y) = \begin{cases} 1 & \dfrac{\mathrm{I}(\mathrm{x},\mathrm{y})}{\prod_{\mathrm{j}=1}^{\mathrm{n}-1}\mathrm{f}_{\mathrm{j}}(\mathrm{x},\mathrm{y})} \geq \dfrac{1}{1+\mathrm{k}^{\mathrm{n}}} \\ 0 & O.W \end{cases} \tag{5}$$

The factorization algorithm is an iterative process that is based entirely on the depth of contrast. The choice of k orders the image into different contrast depth factors. A small value, close to zero, will give large contrast steps and produce a spatially coarse version of the image with relatively few factors, while a value close to unity produces an image version with fine geometrical details with a larger amount of factors.

#198546 - $15.00 USD Received 30 Sep 2013; revised 20 Nov 2013; accepted 21 Nov 2013; published 16 Dec 2013

For each n, the function g_n that represents each pixel in the image is set to be either *1* or *0* according the threshold set by k. This will set the value for the factor f_n. The original image is then divided by the factor f_n and this sets the threshold for the next iteration of g_n. As a result, the first few factors exhibit the largest depth of contrast, and mostly contain the desired image information along with details related to image distortion. Since the desired image information and distortion details generally exhibit different contrast levels, they typically separate into distinct factors, allowing for their differentiation. Random spatial noise usually falls into the higher-order factors, due to their lower contrast levels.

The K-factor algorithm produces a set of contrast-ordered factors, which when multiplied together according to Eq. (3) will reproduce the original image with high fidelity, provided appropriate values of k and M. If, however, the running product is truncated at a lower-order factor f_h, where $h<M$, then those image components with lower contrast levels (i.e., mostly noise) will be de-emphasized in the reconstruction. In addition to noise, the truncated high order factors might also contain some fine spatial information associated with low contrast levels. Thus, we multiply the truncated product by the original image to restore some of these fine spatial details:

$$R_h(x,y) = I(x,y)\prod_{n=1}^{h<M} f_n(x,y) \tag{6}$$

where $R_h(x,y)$ is the truncated reconstruction. The optimal choice of the parameters k and M, as well as the number of factors h in the truncated reconstruction, depends entirely on the nature of the image, rather than on a pre-chosen spatial scale, and therefore it is determined de novo for each application.

Figure 1 illustrates the influence of the K-factor transform on a noiseless image containing two PSFs separated by a distance of $3\sigma\sim600nm$. The K-factor parameters are $k = 0.9$, $M = 48$, $h = 8$. It is clearly seen that the overlap between the two PSFs was reduced.

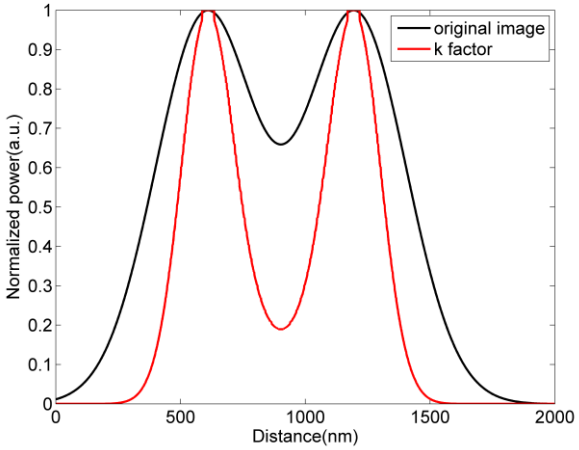

Fig. 1. Image of two PSFs separated by a distance of $3\sigma\sim600nm$. Before the K-factor transform (black) and after the K-factor transform (red).

The proposed technique is an added step during the conventional PALM routine as illustrated in Fig. 2(b). The suggested super-resolved image acquisition technique begins with single frame acquisition using repeated cycles of activation and imaging of the activated fluorophores followed by bleaching to minimize the presence of already visualized particles in posterior acquired images. The frame is passed on to a computer program like MATLAB software package (MathWorks, Natick, MA, USA), where it is applied with the K-factor

#198546 - $15.00 USD Received 30 Sep 2013; revised 20 Nov 2013; accepted 21 Nov 2013; published 16 Dec 2013

algorithm. The next step is the localization of the activated fluorophores using methods of single emitter fitting. Reconstruction and creation of the super-resolved image is done by summing the molecular images across all frames.

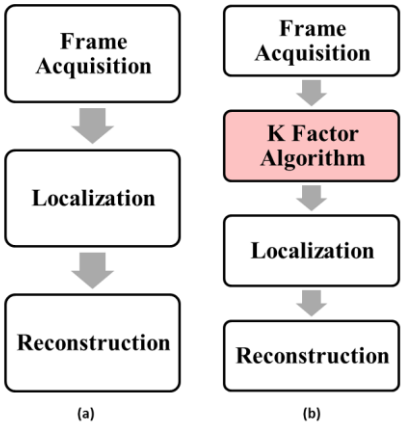

Fig. 2. Super-resolution image acquisition steps for conventional PALM (a) and acquisition steps for the K-factor algorithm (b). Conventional PALM acquisition is divided into three independent steps: frame acquisition using repeated cycles of activation and imaging of the activated fluorophores followed by bleaching to minimize the presence of already visualized particles in posterior acquired images. Localization of the activated fluorophores using methods of single emitter fitting. Reconstruction and creation of the super-resolved image by summing the molecular images across all frames. The K-factor analysis adds a step prior to the localization and is applied to each frame using computer software.

4. Simulation results

To evaluate the performance of the K-factor transformation routine and its impact on localization precision, Monte-Carlo simulations were used to generate mock data sets with two emitters in each set. In these simulations the model was a fluorescence source with $\lambda = 540nm$ that was imaged through an objective lens onto a CCD camera. The model matches the parameter of the Zeiss Axiovert 200 microscope using a *63x* objective, *1.2N.A.* water immersion objective lens. Each pixel on the CCD sensor array had dimensions of $6.45\mu m \times 6.45\mu m$, which translates to $102nm \times 102nm$ in the image plane with the *63x* objective. Background noise was introduced by adding a sample from a Poisson distribution with the parameter N_b. Shot noise was introduced by adding a Poisson distribution with parameter that is the square root of the total intensity of the light at each pixel. The value for σ in the model used for the PSF was calculated from Eq. (2) to be *191nm* for the given imaging parameters.

Gaussian fitting was performed on both the raw simulated data and K-factor filtered data. Each image contained a randomly positioned fluorophore, which was fit using the non linear least-squares minimization routine *lsqnonlin* in MATLAB to fit a model of the form of:

$$I_{psf}(x,y) = \frac{N}{2\pi\sigma^2} e^{-\frac{(x-x_0)^2+(y-y_0)^2}{2\sigma^2}} \tag{7}$$

where N,σ, x_0 and y_0 are all fit parameters. The algorithm initially detected the position of each particle as the pixel with the highest intensity in its region, and preformed a fit by taking 9×9 pixels around this initial location [34]. The fit produces the best estimate of the position of that particular fluorophore, and the process is repeated many times yielding a set of L localization positions $(\hat{x}_i,\hat{y}_i)$ that can be compared with the known positions (x_i,y_i). The root mean square (RMS) localization error is computed for both the raw and K-factor filtered simulated data:

#198546 - $15.00 USD Received 30 Sep 2013; revised 20 Nov 2013; accepted 21 Nov 2013; published 16 Dec 2013

$$err_{rms} = \sqrt{\frac{1}{L}\sum_{i=1}^{L}\left[\left(x_i - x_i\right)^2 + \left(y_i - y_i\right)^2\right]} \tag{8}$$

The position of the each fluorophore, the distance between fluorophores, the number of arriving photons N, the background noise parameter N_b, the K-factor parameter k and the number of harmonics h, were allowed to vary. All analysis was performed in MATLAB.

A crucial aspect is the choice of the parameter k, and thus it was carefully determined after numerous simulations and iterations, to result in a reliable decomposition of the image. The simulated image contained two PSFs separated by $3\sigma \sim 600nm$. The k parameter varied between *0-1*. Additional noise was not introduced in order to reach maximum correlation and maximize the k parameter. For each k value, the maximum correlation between the reconstructed image and the original image was calculated using the *corr* function in MATLAB (as shown in Fig. 3 (left y axis)), and also the number of factors needed for achieving maximum correlation (as shown in Fig. 3 (right y axis)).

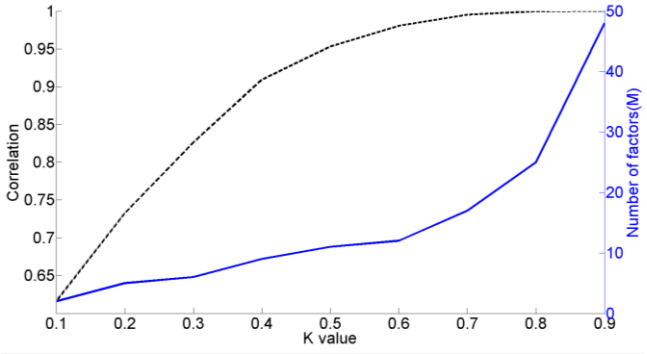

Fig. 3. Maximum correlation between the reconstructed image and the original image of two PSFs separated by a distance of $3\sigma \sim 600nm$, as a function of k values (left y axis). Number of factors needed for maximum correlation as a function of k values (right y axis).

It is clearly seen that for lower k values, the correlation is less than *75%*, and therefore the residual error is relatively large, whereas for higher k values, the correlation can reach *100%*, which means full reconstruction. A value of only $k = 0.9$ yielded a correlation of *100%*; thus a higher k value would not additionally contribute to image reconstruction. It is also evident that the higher the k value, the more factors are required for the full reconstruction, as is predicted by theory, and full image reconstruction results in a longer computation time. Due to this tradeoff between correlation and the overall number of factors, users with computational considerations can choose to work with a lower image correlation, for example a correlation of *95%*, with $k = 0.5$, where the number of factors is only *10*. This will result in a smaller improvement in resolution in the reconstructed image when compared to using a value of $k = 0.9$.

Another key merit is the number of harmonics that the reconstructed image is multiplied by, and its effect on the overlapping of neighboring PSFs. The first factors in the decomposition contain most of the signal's information, where the higher-order factors contain mostly the noise. By multiplying the data with the first harmonics that contain most of the signal data, the signal intensity increases and can be discriminated from the noise. Simulations were carried in order to find the number of harmonics that contain only the signal for different k values. Empirically, the formula that describes the number of harmonics that contains only the signal:

$$h = \frac{1}{6} \times n \tag{9}$$

#198546 - $15.00 USD Received 30 Sep 2013; revised 20 Nov 2013; accepted 21 Nov 2013; published 16 Dec 2013

where n is the number of factors needed for achieving a correlation of *100%* with the original image prior to the decomposition, for a given k. Figure 4(b) presents the influence of the number of multiplied harmonics on the RMS error in localization as a function of distances between centers for $k = 0.9$, $n = 48$. The lowest RMS error was obtained for $h = 8$ calculated according to Eq. (9). The signal information contained in these $h = 8$ factors equals *91%* of the entire signal information. A lower value of h results in a reduced impact of the algorithm, since not all the signal components were enhanced. For the end case of $h = 0$, the reconstructed image equals the original image and the error equals the predicted value for the least squares algorithm [17]. Increasing h also decreases the effect, since both the signal and the noise were enhanced, and the algorithm's influence becomes negligible. For the end case of $h = n$, the error returned is the same as for $h = 0$.

Figure 4(a) illustrates the relation of the K-factor transform and h on overlapping PSFs according to Eq. (9) for a relatively low $k = 0.4$ (red) and for high $k = 0.9$ (blue). In such a scenario, the PSF degradation is due to the overlap of the PSFs with each other, and in order to present the influence of the algorithm on closely spaced PSFs, no additional noise was added. The saddle was reduced by *56.1%* and *54.2%* respectively. However, the lower k distorts the image and reduces the effect of improved localization.

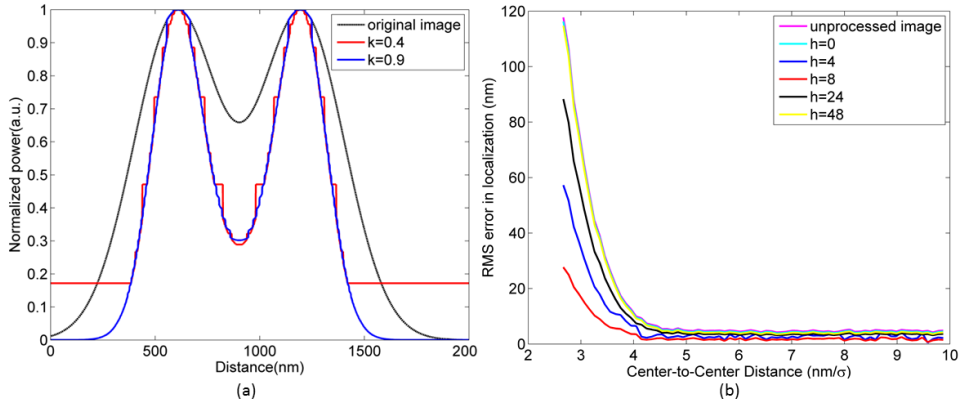

Fig. 4. (a) The K-factor effect on overlapping PSFs for $k = 0.4$ (red) and $k = 0.9$ (blue). (b) the influence of the number of multiplied harmonics on the RMS error in localization as a function of distances between centers for $k = 0.9$, $n = 48$.

The shot noise is a Poisson random process with rate that depends on the total number of photons detected. It is proportional to $\sqrt{N}$, as can be seen in Fig. 5, e.g. an increased number of emitted photons results in a more accurate localization precision [35]. Figure 5 compares the results of the least squares fitting process applied to raw data (black line) and applied to raw data that underwent processing with the K-factor algorithm (red line). It is clearly seen that applying the K-factor algorithm on the raw data followed by the least squares fitting process, resulted in localization error of *~3.5nm* for a high photon count and for a distance of 3σ, an error that is lower than the predicted localization accuracy for the least squares algorithm by itself [17]. The reason for this is due to the influence of the algorithm on the reduction of the σ of each PSF. It narrows the width of the PSF, while allowing for the isolation and localization of overlapping PSFs. For example, in Fig. 4(a), applying the K-factor technique yielded a reduction in σ, by a factor of *1.5*, which results in a localization RMS error that is lower than $\sqrt{N}$.

#198546 - $15.00 USD Received 30 Sep 2013; revised 20 Nov 2013; accepted 21 Nov 2013; published 16 Dec 2013

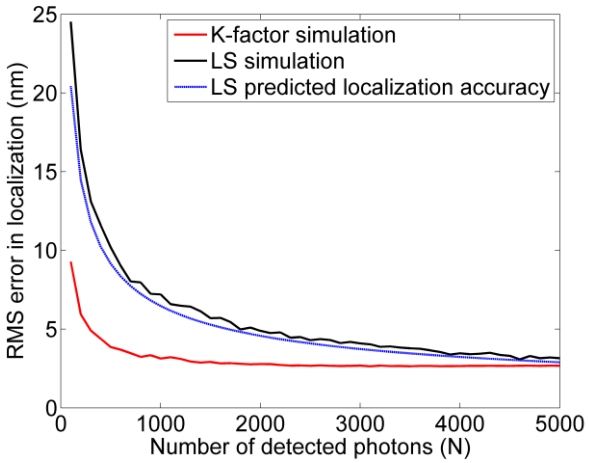

Fig. 5. Error in localization as a function of detected photons, distance between particles *3σ ~600nm*, without background noise. The simulation contained *1000* Monte-Carlo iterations.

The background noise variance for each pixel is a parameter, marked by N_b, that can be measured experimentally and therefore is considered to be known [36], and varied in our simulations between *0* to *10* photons. We calculated the improvement (*%*) in localization error according to:

$$Improvement = 100 \times \frac{RMS_{original} - RMS_{K-Factor}}{RMS_{original}} \tag{10}$$

The results can be seen in Fig. 6. For a distance of *3σ (~600nm)*, at low N_b of *0-2* photons, the improvement was *40-50%*, and with the background increased up to N_b = *10* photons, the improvement reaches up to *85%*. For low photon counts, the improvement in localization accuracy is the most pronounced, and for fluorophores with lower photon yields, such as fluorescent proteins, this will produce the most dramatic improvements in localization accuracy. Since our proposed technique is aimed for reducing noises, the higher the background noise is, the higher the improvement in localization over existing methods. The improvement is achieved due to the high noise discrimination capabilities of the deshadowing algorithm.

#198546 - $15.00 USD Received 30 Sep 2013; revised 20 Nov 2013; accepted 21 Nov 2013; published 16 Dec 2013

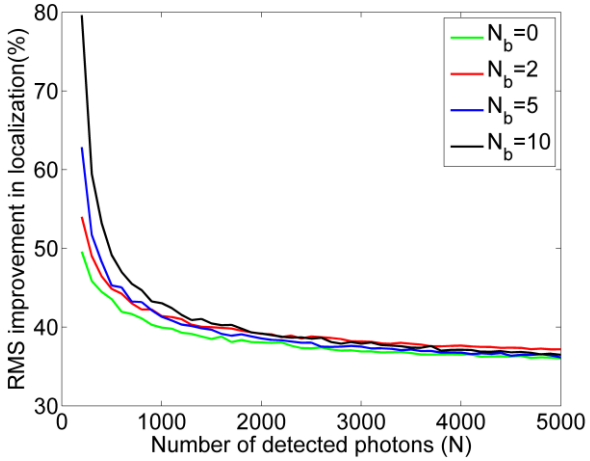

Fig. 6. The improvement in detection using the K-factor algorithm as a function of detected photons, for different background noise photons N_b. The distance between particles was 3σ *~600nm*.

As can be seen in Fig. 7, without background noise, at close distances of *2.5-4.*σ and with a low photon count, the improvement in detection of each spot can reach up to *85%*. At larger distances, the obtained improvement is reduced to *~5-20%*, depending on the photon count.

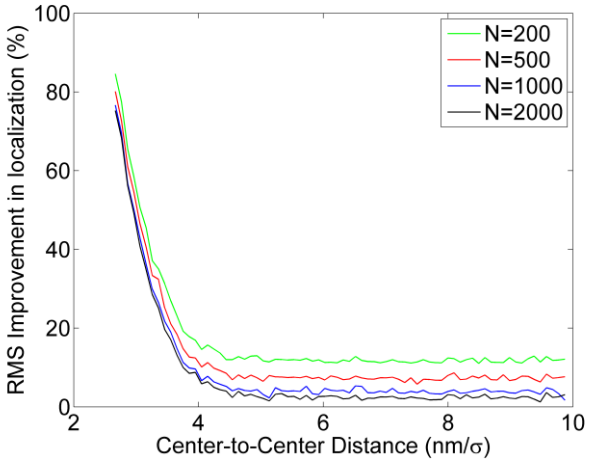

Fig. 7. The improvement in localization using the K-factor algorithm as a function of the distance between florescence centers for different number of photons *N*, without background noise and with $k = 0.9$, $h = 8$.

5. Experimental results

Single molecule imaging experiments were performed in an epi-fluorescence microscope setup consisting of an inverted microscope (Zeiss Elyra P.1, Carl Zeiss Microscopy Inc.), *1.46 N.A.* total internal reflection (TIRF) objective, *642nm* diode laser, and an electron multiplying CCD camera Ixon (897, Andor Technologies PLC.) with EM gain set to *≈200*. The epi-fluorescence filter setup consisted of a dichroic mirror (*650nm*, Semrock) and an emission filter (692/40, Semrock). The sample chamber was mounted in a 3D piezostage (P-737 PIFOC Specimen-Focusing Z Stage, Physik Instrumente). *10,000* images were taken in a TIRF configuration at *40frames/second*. Frames were *512* × *512* pixels with an effective pixel

#198546 - $15.00 USD Received 30 Sep 2013; revised 20 Nov 2013; accepted 21 Nov 2013; published 16 Dec 2013

size of *99.8nm*. The K-factor technique was tested experimentally by imaging microtubules from BSC-1 African green monkey kidney epithelial cells (American Type Culture Collection-ATCC). These cells were cultured and stained with Alexa 647 phalloidin fluorescent probes, using Abcam rat antibody to tubulin, ab6160 as the primary antibody, and Invitrogen Alexa Fluor® 647 Goat Anti-Rat, A-21247 as the secondary antibody. Cell culture methods were standard cell culture techniques for primary/secondary antibody labeling methods. The peak emission wavelength of Alexa 647 is *671nm*. Image pre-processing of the raw data that contained noise filtering and application of the K-factor algorithm on each frame was performed using MATLAB. The localization and the reconstruction of the super-resolved image was done in ImageJ [37] using QuickPALM plugin [38].

The fluorescence data included individual frames in which pairs or larger groups of fluorophores were simultaneously activated and produced a data set with overlapping molecules (Fig. 8(a)). The reconstruction of the final super-resolution PALM image was achieved using extracted data from *10,000* frames. The K-factor method was performed on each of the *10,000* individual frames followed by the same localization and reconstruction procedures to construct a super-resolution image. By applying the K-factor algorithm on each individual frame (Fig. 8(b)), areas with overlapping molecules became distinguishable (Figs. 8(d), 8(f), 8(h)) compared to the original image (Figs. 8(c), 8(e), 8(g)).

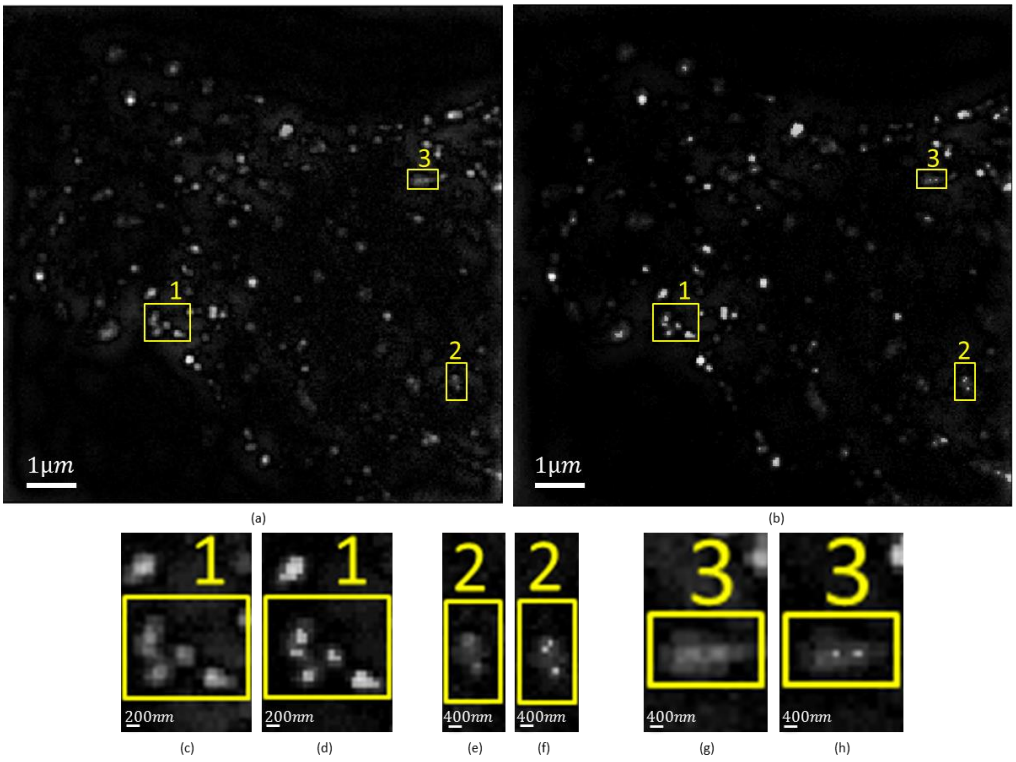

Fig. 8. Individual PALM frame without processing (a) and after K-factor processing(b). Marked regions is where the difference can be clearly seen. (c),(e) and (g) is the magnification of the marked areas in (a). (d),(f) and (h) is the magnification of the marked areas in (b).

The proposed method's performance was tested as follows: first a conventional PALM analysis was performed on the data (Fig. 9(a)), in which frames that contained overlapping emitters were localized (Fig. 9(b)). Subsequently, the K-factor algorithm with parameters of $k = 0.9$, $n = 48$, was applied to the data (Fig. 9(d)) followed by the same single molecule fitting technique (Fig. 9(e)). As can be seen from the fitting process using both the conventional

#198546 - $15.00 USD Received 30 Sep 2013; revised 20 Nov 2013; accepted 21 Nov 2013; published 16 Dec 2013

PALM and the K-factor algorithm in (Fig. 9(b) and 9(e)), when neighboring molecules were in close proximity, like in the upper section of the image, the K-factor routine enabled the identification of two overlapping molecules, whereas in its absence, only one molecule was identified. Figure 9(c) and 9(f) show the cross section of the dashed line that passes through the center of the overlapping two emitters with $\sigma = 195nm$ in the upper part of the image of Fig. 9(b) and 9(e) respectively. As can be seen, applying the proposed method prior to the localization reduces the saddle of overlapping PSFs and enables their localization.

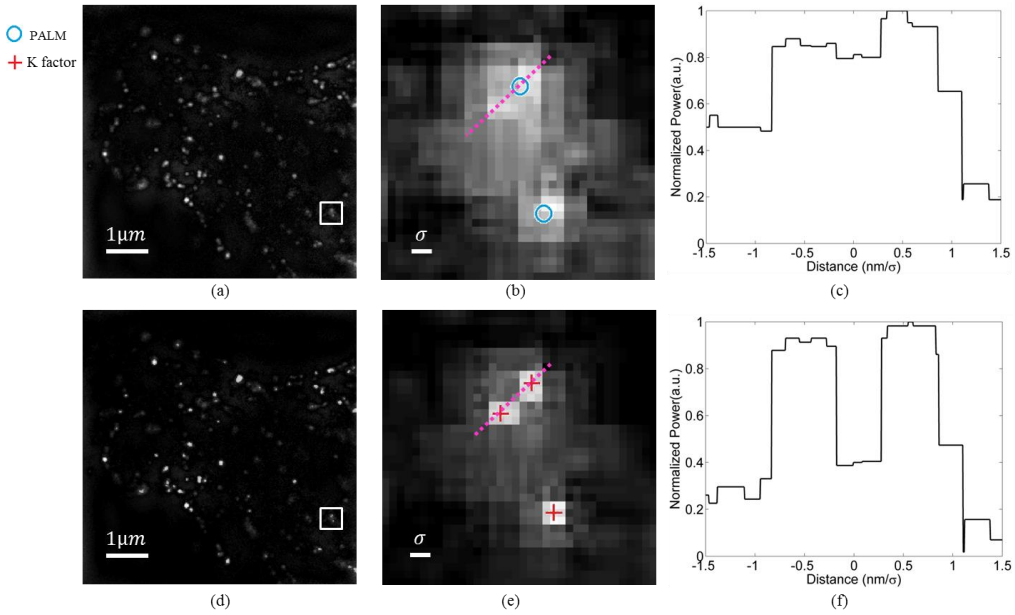

Fig. 9. Single molecule fitting process preformed on individual frames of conventional PALM (Upper row) and on frames preprocessed by the K-factor algorithm (Lower row). (b) is the magnification of the marked area in (a). PALM analysis (blue circles) localize 2 emitters. (e) is the magnification of the marked area in (d). K-factor preprocessing followed by PALM analysis (red crosses) localize 3 emitters. (c) and (f) show the cross section of the dashed line that passes through the center of the overlapping two emitters with $\sigma = 195nm$ in the upper part of the image in (b) and (e) respectively.

In order to create the fully reconstructed image, all the single emitter estimations of individual frames were summed, using both the unprocessed images and the K-factor processed images. The use of the K-factor algorithm enabled the extraction of data that otherwise would have been discarded from each frame, which resulted in the ability to reconstruct the full image with fewer frames than the conventional PALM image. To quantify the reduction in number of frames that require the full reconstruction using the K-factor process, an iterative approach was used. First, the correlation coefficient between the two images was calculated for a total number of *10,000* frames used for the reconstruction. Then, for this given correlation coefficient, the number of frames in the K-factor reconstruction process was reduced, until the point where the correlation coefficient decreased by *5%*. This was set to be the lowest number of frames needed for the full reconstruction in comparison to the conventional PALM.

Using the K-factor algorithm, only 5,735 frames were required for the full reconstruction of the image (Fig. 10(b)) whereas conventional PALM analysis required 10,000 (Fig. 10(c)). Taking only 5,735 frames using the conventional PALM produced a less detailed image estimation with gaps in locations where there was a high density of overlapping emitters (Fig. 10(a)). Taking 10,000 frames using the K-factor algorithm resulted in a sharper image estimate, due to the higher accuracy in localization (Fig. 10(d)).

#198546 - $15.00 USD Received 30 Sep 2013; revised 20 Nov 2013; accepted 21 Nov 2013; published 16 Dec 2013

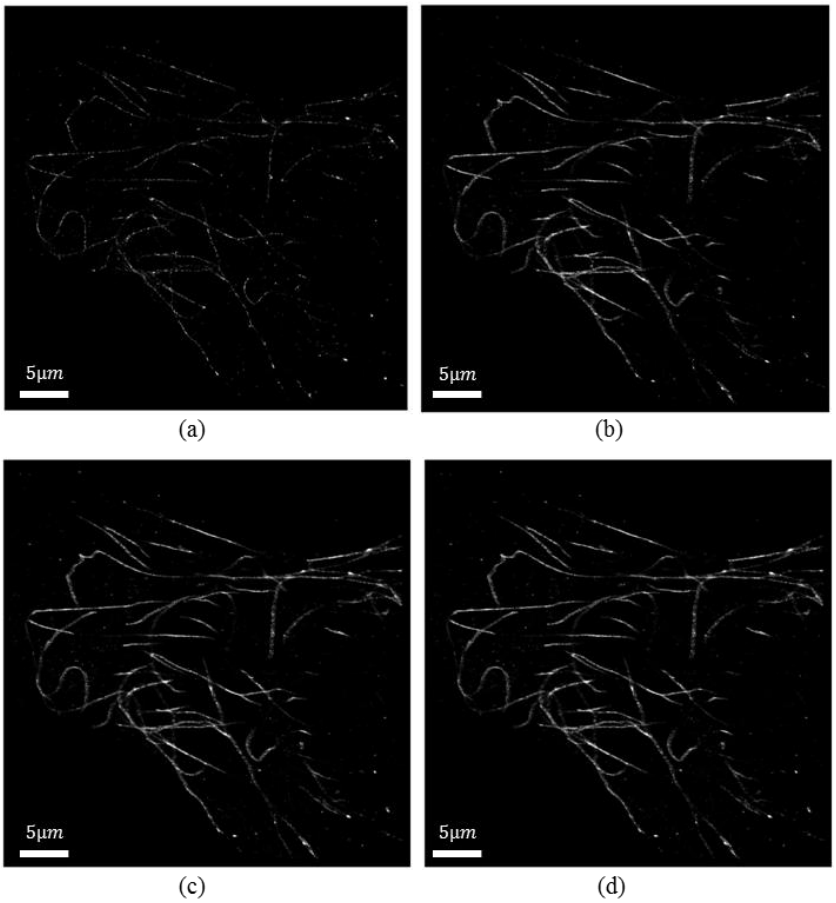

Fig. 10. Reconstruction of imaging data from Alexa647 labeled microtubules sample without processing and using the K-factor algorithm prior to the localization. Images in the upper row represent reconstructed image using *5,735* frames and those in the lower row represent reconstructed image using *10,000* frames. (a,c) conventional PALM analysis. (b,d) K-factor algorithm applied to raw data followed by conventional PALM analysis.

The effective resolution of the reconstructed image was measured using the method of Fourier ring correlation (FRC) [23,39]. FRC evaluates the degree of correlation of two independent reconstructions of the same object in frequency space and determines the resolution threshold (the spatial frequency) at which both reconstructions are consistent and considered to be resolved. Reconstruction using *10,000* individual frames without additional processing resulted in effective resolution of *55.74nm*, whereas taking the same amount of frames and using the K-factor algorithm additional processing yielded a resolution of *43.21nm*. When taking only *5,735* frames, the resolution obtained without additional processing was *80.16nm*, compared to *55.15nm* with the K-factor algorithm processing. The use of the proposed method in comparison to conventional PALM analysis improves the resolution of the obtained image. In addition, the same effective resolution of a given super-resolution image can be obtained using the proposed method with a lower number of frames, and as a result, decreases image acquisition time while increases the sampling density. For the experimental results presented, acquisition of each frame of an Alexa647 labeled microtubules image with a field of view: $51.1\mu m \times 51.1\mu m$ takes *40ms*. For an effective resolution of *~55nm*, the amount of individual frames required for the generation of the super-resolution image was *10,000* using conventional PALM, in comparison to *5,735* individual

#198546 - $15.00 USD Received 30 Sep 2013; revised 20 Nov 2013; accepted 21 Nov 2013; published 16 Dec 2013

frames using the K-factor algorithm. The use of the K-factor processing enabled the decrease of *42%* of the total super-resolution image acquisition time for the same resolution. The penalty is the increase in processing time, which is *0.3ms* per frame in a simple PC (HP Compaq Elite 8300 Microtower PC with Windows 7 professional 64 bit operation system, Intel® Core i5-3470 processor, 3.20 GHz, 12 GB RAM).

6. Conclusions

Implementation of an image decomposition K-factor algorithm on images acquired by fluorescence microscopy techniques like PALM and STORM, prior to the fitting process, allows for the analysis of images with a higher density of activated fluorophores per frame, thereby offering an increase in the image acquisition speed. In addition, it can improve the precision of localization of individual fluorophores.

The proposed method was compared to localization performed by standard methods of single molecule fitting, such as least-squares fitting and maximum likelihood. In the simulation section, data fitting was performed using the method of least-squares, while in the experimental section, the fit was performed using both methods. The technique showed maximum impact and effect on closely spaced fluorescent spots, such as two neighboring PSFs overlaping extensively. This paper examined the effects of changing the parameters of the K-factor algorithm, such as the depth of contrast *k*, the number of factors needed for achieving maximum correlation for a given *k* and the number of harmonics as a function of the distance between particles, the number of arriving photons and the background noise parameter.

The best way to appropriately choose parameters for working with the K-factor algorithm is first determine the *k* parameter that yields the best reconstruction of the image in terms of maximum correlation, and subsequently derive the parameters *n* and *h*. Our validation studies using simulated and experimental data showed that the K-factor algorithm can increase image collection time of super-resolution data by *42%* while maintaining the same image resolution, or improve the obtained resolution by *37%* for the same total super-resolution image acquisition time (provided the sample still has active fluorophores). Therefore, the method can be a useful tool for fast single molecule fitting super-resolution microscopy techniques operating at high density, allowing for an increase in activated fluorophore density (in units of μm^{-2}) of *~50%*.

When comparing the performance of the K-factor algorithm to the two multi-emitter fitting methods presented in the introduction section, both techniques – utilizing a maximum likelihood technique for GPU analysis and statistical deconvolution – do not improve the obtained resolution of the super-resolution image as does the K-factor method, and are aimed at reducing the number of frames needed for acquisition by factor of *~5* and *~8* respectively. The multi-fitter method has an analysis times on the order of minutes, similar to the K-factor, whereas the statistical deconvolution method requires *~10* times more computation *time/frame* than standard methods of single-emitter fitting, and in total does not decrease image acquisition time, as the K-factor technique does.

Acknowledgments

This work was supported by NSF grant CAREER #DBI-0845193 and NIH grant R01 NS034307. We would also like to thank Edward J. Hujber for his help with imaging and data collection.